CHAPTER–4A

Bis(pyridyl)-di-imines as Ratiometric Chemosensor for Ni(II) and Cd(II) Ions

Bis(pyridyl)-di-imines as Ratiometric Chemosensor for Ni(II) and Cd(II) Ions

4A.1 Introduction

Massive industrial pollution leading to an uncontrolled amount of transition metal ions in our surroundings is linked to health hazards and environmental degradation.[1] Among the various transition metals, the presence of cadmium in the environment has been an increasing concern as it possesses detrimental effects on human health. Cadmium has several industrial applications, which include its use in alloys, electroplating, dry-cell batteries, and through different ways, it enters the environment. Similarly, nickel is used as pigment in paints, the catalyst for hydrogenation, magnetic tapes, electroplating, etc.[2] Nickel is also an essential nutrient for the biological systems involving the enzymes of some micro-organism and plants,[3] however, an excess amount of nickel is known to cause severe health issues like cancer, asthma, and acute pneumonitis.[4]

There has been widespread research in the design and synthesis of new molecular systems with distinguished capabilities of recognizing and sensing metal ions as it will address the environmental concern of metal toxicity[5] as well as the issue of the presence of essential elements in biological systems.[6] Metal ion detection techniques can be classified into two categories: (i) Indirect detection based on the molecular system and (ii) Direct detection based on instruments (Figure 4A.1). Although several analytical methods, such as Atomic Absorption Spectroscopy (AAS),[7] Flame Atomic Absorption Spectrometry-Electro Thermal Atomization (FAS-ETA),[8] Inductively Coupled Plasma Atomic Emission Spectroscopy (ICP-AES),[9] for detection of metals are available, still, there is a need for designing sensors which will be able to work in a relatively simple, fast and cost effective manner. Fluorescence sensor,[10] chemosensor,[11] colorimetric sensor,[12] ratiometric sensor,[13] potentiometric sensor[14] have emerged as important tools because of their high selectivity, sensitivity in detecting metal ions

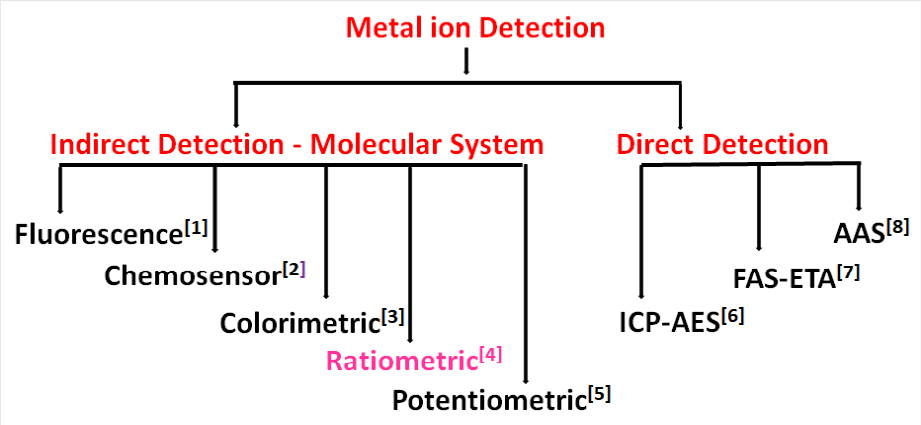

Figure 4A.1: Classification of metal ion detection techniques

and are a comparatively inexpensive method to detect heavy metal ions. Although a large number of research papers deal with these sensors for detecting metal ions, very few reports are available in the literature regarding the detection of nickel and cadmium.

Ag_2S-Cd mixture, cadmium chelates, tetrol, macrocycles, and a variety of other ionophores are exploited widely as potentiometric sensors for detecting cadmium.[15] Dithiazone based potentiometric electrode sensor was reported to have determined trace amount of Cd(II) ions in environmental soil and water samples, with detection limit 1×10^{-7} M L^{-1}. Dibenzocyclam nickel,[16] Schiff base membrane in PVC,[17] dibenzo-18-crown-6 in PVC,[18] heterogeneous membranes of porphyrins, ion exchangers are used as nickel selective potentiometric sensor. The disadvantages involved in these techniques include limited working concentration range of the electrodes and membranes, poor selectivity, low response, and an overall time-consuming technique.

Colorimetric chemosensor is an inexpensive method where the observation directly proceeds through the naked eye and doesn't require any equipment. In this technique, the pre-treatment of the sample is required but the sensor is not regenerated. Researchers have focused majorly on fluorescence sensor as it is a fast response probe. The quenching or enhancing fluorescence of the probe can be utilized for sensing. The drawbacks associated with fluorescence sensors may involve poor solubility of the probe, low sensitivity, lack of selectivity, quenching nature, serious interference from other metal ions, and the requirement of UV-vis radiation to analyze the observation.

A fluorescent sensor based on boron-dipyromethane has been reported, which quenched 95% of fluorescence upon addition of Ni(II) ion in acetonitrile and the reverse was observed in triethanolamine.[19] An optical chemical sensor based on thiazolo-trizol derivative was reported for detecting the Ni^{+2} in PVC matrix by Aksuner and coworkers. This optical sensor showed a detection limit of 8.5×10^{-10} M for Ni(II). Further, the membrane has a very good selectivity towards Ni(II) ion over a wide variety of other metal ions in solution and gave good results for applications in direct determination of Ni(II) in real samples that are satisfactorily comparable with corresponding data using flame atomic absorption spectrometry.[20] A thiazole functionalized fluorogenic ionophore synthesized by Gupta showed fluorescence responses towards various metal ions. The sensor showed high selective and sensitive electrochemical and fluorescence response towards Ni^{+2} in the presence of various competing metal ions. This

fluorescence chemosensor is easily detectable by the naked eye with a high association constant 1.07×10^4 M^{-1}.[21]

In order to understand the role of nickel in biological systems, researchers have developed various Ni^{+2} -selective fluorescent indicators. Chang et al., have reported a turn-on fluorescent sensor for the selective detection of Ni^{+2} in water and biological samples.[22] The fluorescent sensor showed a 25-fold fluorescence increase upon binding with Ni^{+2} and is effective in monitoring the changes in Ni^{+2} levels within biological systems. Prabhu and co-workers developed a highly selective fluorescent chemosensor based on pyrene-conjugated pyridine for nickel ion. The ratiometric sensing of nickel ions by the chemosensor is due to the formation of monomer-excimer species and it was effective in detecting the Ni^{+2} ion in biological samples.[23] Recently, Goswami group also developed a ratiometric chemosensor based on quinoxaline derivative, which showed naked eye detection for Ni^{+2} ion.[24]

Wang and co-workers reported a dual-emission quantum dot (QD) nanohybrid for fluorescence ratiometric determination of cadmium ions (Cd^{2+}) in water samples, where the "turn-on" model and "ion-imprinting" technique have been incorporated simultaneously. The nanohybrid probe was composed of green-emitting CdSe QDs that covalently linked onto the surface of silica nanoparticles embedded with red-emitting CdTe QDs.[25] Bao and co-workers synthesized a ratiometric fluorescent sensor for Cd^{+2}. Being in the same group, Cd and Zn, have similar chemical properties, but they have different roles in the environment as well as biological systems. The sensor synthesized by Bao and co-workers can distinguish Cd^{+2} from Zn^{+2} where the sensor on interaction with Cd^{+2} showed enhanced fluorescence intensity and bathochromic shift of peak maxima. The detection limit is down to nanomolar range concentration in an aqueous solution.[26] Many researchers have also utilized the Schiff base molecular systems as a receptor for chemosensors. Li et al., have developed a fluorescent chemosensor based on Schiff base, which has hydroxynaphthalene and indole moieties, for selective detection of Zn(II) in an aqueous solution.[27] Li et al., have constructed Zn-Ni heterotrinuclear complex of a symmetrical Schiff base ligand bis(acetylacetone)ethylenediamine, which functioned as a selective luminescent probe for the Ni^{+2} ion.[28] Jiang et al., have reported a colorimetric chemosensor, synthesized from coumarin derived Schiff base capable of sensing Ni^{+2} ions.[29]

In this chapter, we have reported a Schiff Base, (1E,1'E)-*N,N'*-(butane-1,4-diyl)bis(1- (pyridin-2-yl)methanimine), **L3c**, as a chemosensor for cadmium and nickel (Scheme 4A.1) among the various di-imines. Our group has previously reported the photophysical properties of a series

of Schiff bases including **L3c** and correlated the observed AIE behavior with their crystal structure.[30] In 2015, Mendoza et al., have reported a nickel complex of **L3c**,[31] where **L3c** also acted as an ionophore sensor for cadmium in polymeric membrane electrodes. Complexation studies of Mn^{+2}, $Cd^{+2,}$ and Zn^{+2} ions with **L3c** were done by NMR technique using ^{7}Li nucleus as a probe.[32] Based on these observations, it is expected that **L3c** may act as a metal ion sensor, which has been effectively analyzed using photophysical measurements. The following points are investigated in the present work: (i) Metal ion sensing property of **L3c** with various metal ions; (ii) Estimation of the binding ratio of metal ions with **L3c** using mole ratio method;[33] (iii) Determination of binding constant from Yoe Jone's method[34] and 'limit of detection'(LOD) of metal ions; (iv) effectiveness of **L3c** as a sensor for Ni(II) and Cd(II) over other di-imines; (v) Study of molecular interaction between **Cd(II)-L3c** from NMR spectra and and **Ni(II)-L3c** from crystal structure analysis. (vi) Analysis of the complexation of **L3c** with Cd(II) and Ni(II) from SEM and EDS. (vii) Real time application of **L3c** in detection of nickel ion using river water.

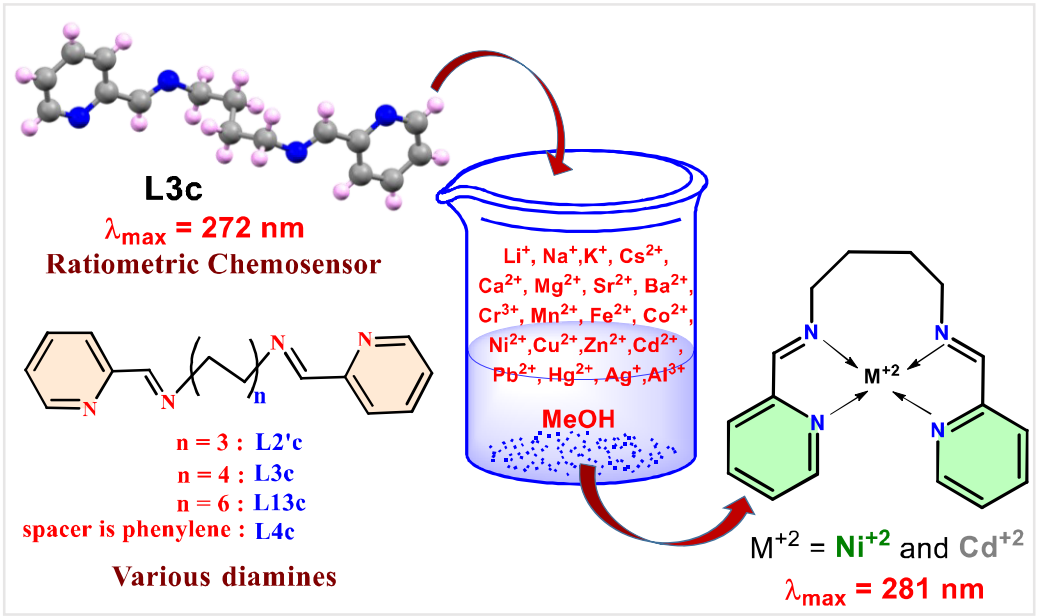

Scheme 4A.1: Metal ion sensing property of **L3c**

4A.2 Experimental

4A.2.1 General

Infra-red spectra were obtained from Shimadzu model-00247, IRAffinity-1S. UV-Visible spectra and Fluorescence Spectra were recorded on Jasco V-650 Spectrophotometer and Fluorimax-4 0426C-0809, respectively. Proton and Carbon-13 Nuclear Magnetic Resonance (^{1}H and ^{13}C NMR) spectra were recorded on a 400 MHz spectrophotometer (Bruker). Powder

X-Ray Diffraction (PXRD) were recorded with a Rigaku miniflex ll, λ =1.54, Cu Kα. Agilent 6545 Q-TOF LC/MS is used for ESI-HRMS. 1×10^{-3} M of stock solution is prepared for all spectral analysis using methanolic solution (MeOH:MeOH (v/v)), pH of **L3c** (0.25×10^{-4} M) = 7.54, pH of $NiCl_2$ (0.25×10^{-4} M) = 6.94, pH of $CdCl_2$ (0.25×10^{-4} M) = 7.28. pH study was carried out in acetic buffer using acetic acid and sodium hydroxide. Atomic absorption spectra (AAS) were measured using AA-7000, Shimadzu. Scanning electron microscope (SEM) and electron dispersive spectroscopy (EDS) analysis were done by Leica Ultra Microtome EMUC7, Apreo LoVac model with Aztec Standard EDS system-resolution 127 eV on Mn-Kα.

4A.2.2 Synthesis of ligands and complexes

The compounds **L3c, L2′c L4c** and **L13c** were synthesized by the usual method of preparation of Schiff bases, which involved the condensation reaction of primary diamines with an aldehyde precursor in alcoholic solution under reflux conditions.

4A.2.2.1 (1E,1'E)-*N*,*N*′-(butane-1,4-diyl)bis(1-(pyridin-2-yl)methanimine) (L3c)[30]

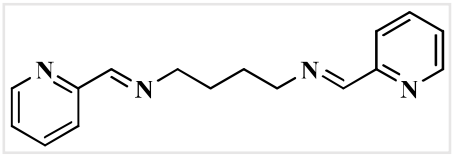

1,4-Diaminobutane (0.5 mL, 10 mmol) was added dropwise to a solution of 2-carboxaldehyde pyridine (2.3 mL, 20 mmol) in ethanol (40 mL). The mixture was refluxed at 80 °C for 6 hours. The solvent was removed under vacuum and the green color semi-solid product was recrystallized with hexane. Yield: 43%; melting point: 73.5 °C; IR (cm^{-1} KBr pellet): 3055(w), 3009(w), 2916(s), 2839(s), 1636(vs), 1566(s), 1466(vs), 1435(vs), 1366(m), 1335(s), 1288(w), 1211(w), 1188(w), 1142(w), 1088(w), 1041(s), 987(vs) (Figure A-61). ^{1}H NMR (400 MHz, $CDCl_3$) δ ppm: 8.61 (ddd, *J* = 4.8, 1.7, 0.9 Hz, 2H), 8.36 (s, 2H), 7.95 (dt, *J* = 7.9, 1.0 Hz, 2H), 7.73–7.69 (m, 2H), 7.28 (ddd, *J* = 7.5, 4.9, 1.2 Hz, 2H), 3.71 (td, *J* = 5.2, 1.4 Hz, 4H), 1.83–1.78 (m, 4H) (Figure A-62). ^{13}C NMR (100 MHz, CDCl3) δ ppm: 161.88, 154.46, 149.35, 136.47, 124.58, 121.18, 77.32, 77.00, 76.68, 61.18, 28.38 (Figure A-63). HRMS: m/z calcd for $C_{16}H_{18}N_4$ (M^+) = 266.15, found 267.1606 (Figure A-64).

4A.2.2.2 (1E,1'E)-*N*,*N*'-(propane-1,3-diyl)bis(1-(pyridin-2-yl)methanimine) (L2′c)[35]

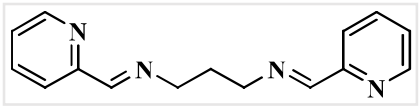

1,3-Diaminopropane (0.5 mL, 10 mmol) was added dropwise to a solution of 2-pyridinecarboxaldehyde (2.3 mL, 20 mmol) in ethanol (40 mL). The mixture was refluxed

at 80 °C for 6 hours. The solvent was removed under vacuum and the orange color semi-solid product was recrystallized with ethanol-water (5:1). Yield: 50%; melting point: 41 °C; IR (cm^{-1} KBr pellet): 3055(w), 1643(s), 1581(m), 1465(s), 1365(w), 1296(w), 1049(w), 771(vs), 665(w) (Figure A-65). ^{1}H NMR (400 MHz, $CDCl_3$) δ ppm: δ 8.66 (ddd, *J* = 4.8, 1.6, 0.9 Hz, 2H), 8.44 (s, 2H), 8.03 (s, 2H), 7.74 (s, 2H), 7.33 (dd, *J* = 2.6, 1.2 Hz, 2H), 3.84 – 3.80 (m, 4H), 2.19 (p, *J* = 6.9 Hz, 2H) (Figure A-66). ^{13}C NMR (100 MHz, CDCl3) δ ppm: 162.28, 149.42, 136.53, 124.67, 121.25, 59.00, 31.69 (Figure A-67). HRMS: m/z calcd for $C_{15}H_{16}N_4$ (M^+) = 252.14, found 253.1450 (Figure A-68).

4A.2.2.3 (1E,1'E)-*N*,*N*'-(hexane-1,6-diyl)bis(1-(pyridin-2-yl)methanimine) (L4c)[36]

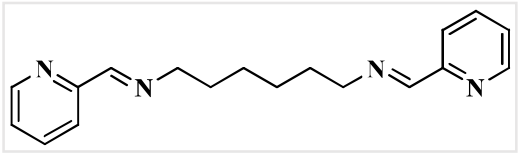

Hexamethylenediamine (0.5 mL, 10 mmol) was added dropwise to a solution of 2-pyridinecarboxaldehyde (2.3 mL, 20 mmol) in ethanol (40 mL). The mixture was refluxed at 80 °C for 6 hours. The solvent was removed under vacuum and the brown color semi-solid product was recrystallized with ethanol-water (5:1). Yield: 49%; melting point: 45 °C; IR (cm^{-1} KBr pellet): 2931(s), 1643(s),1581(m), 1465(s), 1436(s), 1334(m), 1149(w), 987(m), 771(vs), 655(w) (Figure A-69). ^{1}H NMR (400 MHz, $CDCl_3$) δ ppm: δ 8.63 (dd, *J* = 4.8, 0.6 Hz, 1H), 8.37 (s, 1H), 7.98 (d, *J* = 7.9 Hz, 1H), 7.79 – 7.64 (m, 1H), 7.32 (dd, *J* = 4.9, 1.2 Hz, 1H), 3.79 – 3.60 (m, 2H), 1.85 – 1.62 (m, 2H), 1.50 – 1.40 (m, 2H). (Figure A-70). ^{13}C NMR (100 MHz, CDCl3) δ ppm: 161.74, 154.55, 149.35, 136.58, 124.62, 121.21, 76.74, 61.45, 30.61, 27.12 (Figure A-71). HRMS: m/z calcd for $C_{18}H_{22}N_4$ (M^+) = 294.18, found 295.1901 (Figure A-72).

4A.2.2.4 (1E,1'E)-*N*,*N*'-(1,4-phenylene)bis(1-(pyridin-2-yl)methanimine) (L13c)[37]

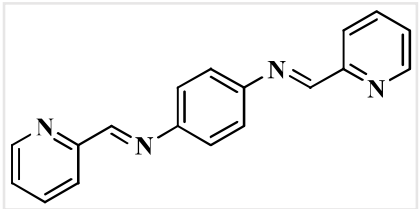

p-Phenylene diamine (1.08 g, 10 mmol) was added dropwise to a solution of 2–pyridnecarboxaldehyde (2.3 mL, 20 mmol) in ethanol (40 mL). The mixture was refluxed at 80 °C for 6 hours. The solvent was removed under vacuum and the yellow solid product was recrystallized with methanol. Yield: 52%; melting point: 153 °C; IR (cm^{-1} KBr pellet): 2931(m), 1612(s), 1489(m), 1458(s), 1427(s), 1350(m), 1226(w), 987(m), 840(vs), 632(m) (Figure A-73). ^{1}H NMR (400 MHz, $CDCl_3$) δ ppm: δ 8.74 (d, *J* = 4.5 Hz, 2H), 8.67 (s, 2H), 8.23 (d, *J* = 7.9 Hz, 2H), 7.84 (t, *J* = 7.7 Hz, 2H), 7.39 (s, 6H) (Figure A-74). ^{13}C NMR (100 MHz, CDCl3) δ ppm: 160.20, 154.58, 149.76, 149.56, 136.71, 125.17, 122.24, 121.97 (Figure A-75).

4A.2.2.5 Synthesis of Cd(II)-L3c complex

A mixture of $CdCl_2$ in hot acetonitrile was added to a solution of the ligand **L3c**, in 10 mL of dichloromethane. The mixture was refluxed at 40 °C for 24 hours. The residue was filtered from the mixture under vacuum affording grey solid for **Cd(II)-L3c**. Yield: 85%; melting point: 311 °C; IR (cm^{-1} KBr pellet): 3394(m), 3068(w), 1649(s), 1591(s), 144(s), 1342(m), 1309(s),1195(m), 1014(s), 756(s), 638(m) (Figure A-76). HRMS: m/z calcd for $C_{16}H_{18}CdClN_4$ (M^+) = 415.02, found 415.0247(Figure A-77).

4A.2.2.6 Synthesis of Ni(II)-L3c complex

A mixture of $NiCl_2.6H_2O$ in hot acetonitrile was added to a solution of the ligand **L3c**, in 10 mL of dichloromethane. The mixture was refluxed at 40 °C for 24 hours. The residue was filtered from the mixture under vacuum affording green solids for **Ni(II)-L3c**. Yield: 89%; melting point: (230-237) °C; IR (cm^{-1} KBr pellet): 3167(m), 3022(m), 1645(m), 1595(s), 1568(w), 1442(m), 1377(m), 1305(m), 1151(m), 1041(w), 985(w), 783(s), 642(w) (Figure A-78). HRMS: m/z calcd for $C_{16}H_{18}NiClN_4$ (M^+) = 359.06, found 359.0565 (Figure A-79).

4A.2.3 Method for preparation of standard calibration curve for determination of Ni (II) ion by L3c using UV-visible analysis

1 mL of 1×10^{-4} M, 2×10^{-4} M, 3×10^{-4} M, 4×10^{-4} M and 5×10^{-4} M of Ni^{+2} solution (pH ~ 7) and 0.5 mL of 10^{-3} M (pH ~ 7.2) of **L3c** were taken in a separate 5 glass vials. For each vial, 2 mL volume was made up using triple distilled water. The solutions were kept for 5 minutes and then monitored by UV-visible Spectrophotometry. The standard calibration curve was plotted (Figure A-80).

4A.2.4 Method for determination of nickel ion in river water by L3c using UV-visible analysis

1 mL of 1×10^{-4} M, 2×10^{-4} M, 3×10^{-4} M, 4×10^{-4} M and 5×10^{-4} M of Ni^{+2} solution (pH ~ 7) and 0.5 mL of 10^{-3} M (pH ~ 7.2) of **L3c** were taken in a separate 5 glass vials. For each vial, 2 mL volume was made up using the river water. The solutions were kept for 5 minutes and then monitored by UV-Visible Spectrophotometry. From the standard calibration curve (Figure A-80), the concentration corresponding to five different absorbances was determined (Figure A-81).

4A.3 Results and discussion

4A.3.1 UV-Visible absorption spectra of L3c in presence of metal ions

UV-Visible absorption spectra were recorded to analyse the metal ion sensing property of **L3c**. The molecule **L3c** has a small chromophoric moiety and showed absorption maxima at 234 nm ($\pi \rightarrow \pi^*$) and 272 nm ($n \rightarrow \pi^*$).[38] The addition of metal salts ($LiCO_3$, NaCl, KCl, $Mg(NO_3)_2$, $Ca(Cl_2)$, $Sr(NO_3)_2$, $Ba(Cl_2)_2$, $CsCO_3$, $CrCl_3$, $FeSO_4$, $Mn(Cl_2)_2$, $Co(NO_3)_2$, $Ni(NO_3)_2$, $Cu(NO_3)_2$, $Zn(NO_3)_2$, $Cd(Cl_2)_2$, $Pb(NO_3)_2$, $AgNO_3$, $Al(OH)_3$) into **L3c** solution in 1:1 (**L3c**: metal salt) and resulted in red shift of $n \rightarrow \pi^*$ peak for Cd(II) and Ni(II), while no shift in peak position was observed for other metal salts (Figure 4A.2a, Figure A-82).

A bathochromic shift was observed in $n \rightarrow \pi^*$ peak on adding Cd(II) and Ni(II) salts (Figure 4A.2a) in **L3c**. This suggest that the coordination of Cd(II) and Ni(II) to **L3c** resulting in intra Molecular Charge Transfer (ICT).[29] The absorption changes due to the complexation with Cd(II) and Ni(II) with **L3c** can be explained in terms of charge-dipole interaction. The binding of the metal centre with pyridyl-N and imine-N resulted in more stabilization of the excited state compared to the ground state. A plot of Absorbance (at absorption maxima for $n \rightarrow \pi^*$) vs. different metal ions showed maximum absorbance for Cd(II) and Ni(II) compared to other metal ions (Figure A-83).

4A.3.2 IR spectra analysis to determine the binding of Ni(II) and Cd(II) to L3c

Coordination of Ni(II) and Cd(II) with **L3c** is also indicated by the IR spectrum. Free **L3c** showed IR peaks at 1637 cm^{-1} for C=N and 1585 cm^{-1} for C=C, while the IR spectra of 1: 1 (**L3c**: metal salt) showed the corresponding peaks at 1648 cm^{-1}, 1591 cm^{-1} for Cd(II) and 1644

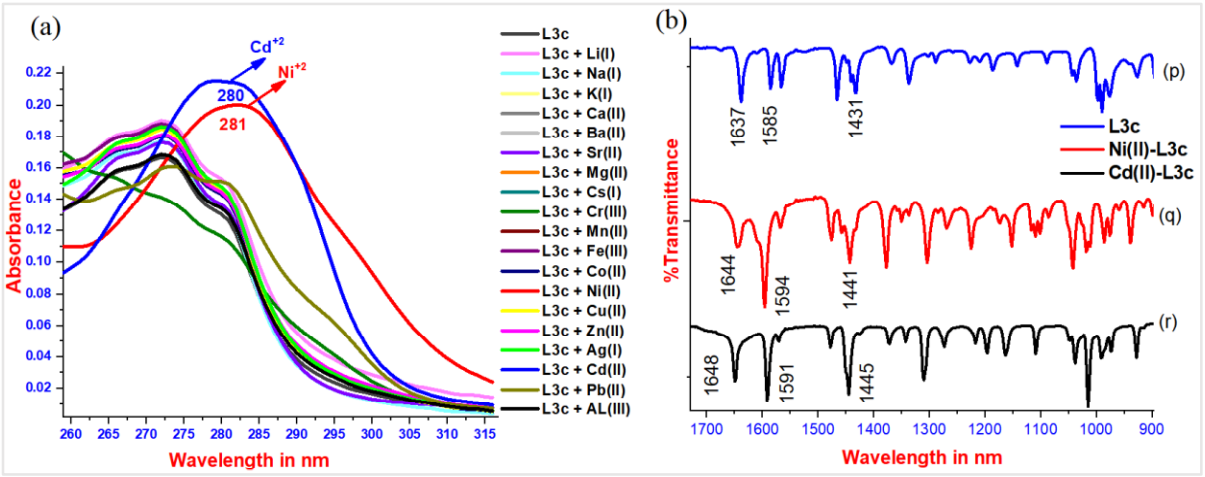

Figure 4A.2: (a) UV-Visible absorption spectra of **L3c** with different metal salts in 1:1 ratio, IR spectrum of (a) **L3c**, (b) 1: 1 (**L3c**: Ni^{+2}), (c) 1: 1 (**L3c**: Cd^{+2})

cm^{-1}, 1594 cm^{-1} for Ni(II) (Figure 4A.2b). The shifting of peak positions can be explained on the basis of change in C=N and C=C bond strength on chelation of Cd(II)/Ni(II) with **L3c**. The ring strain associated with chelation may be the reason for higher wavenumber for C=N and C=C than in free **L3c**. Also, in free **L3c**, the extent of delocalization of electron density[23] is much more than when it is chelated with some metal.

4A.3.3 Mole ratio method to evaluate the binding mode of L3c with Ni(II) and Cd(II)

The UV-visible absorption spectra clearly indicates the preference of **L3c** to bind to Ni(II) and Cd(II) over other metal ions (Figure 4A.2a). Mole ratio method is used to determine the binding mode of **L3c** with Ni(II) and Cd(II). In mole ratio method, the concentration of **L3c** was kept constant at 0.5×10^{-4} M and UV-visible spectrophotometric titration was performed by using 10^{-3} M stock solution of Ni(II)/Cd(II). For each titration, the total volume was maintained as 2 mL, where 1 mL of 0.5×10^{-4} M **L3c** was taken, 10^{-3} M of Ni(II) solution ranging from 0 to 170 μL was added and rest of the volume was made up using MeOH. UV-Visible absorption spectra were recorded for each solution and it was observed that on increasing the Ni(II) concentration, red shift of $n \rightarrow \pi^*$ peak was observed (Figure 4A.3a, Figure A-84). The plot of absorbance (of $n \rightarrow \pi^*$ peak) vs. volume of Ni(II) solution showed that the saturation in absorbance was reached at 50 μL of Ni(II) solution, which is equal to 0.5×10^{-4} M of Ni(II) solution. From figure 4A.3b, the binding mode of **L3c** with Ni(II) is found to be 1:1. The UV-Visible titration of **L3c** with Cd(II) showed the formation of 1:1 stoichiometric complexation (Figure 4A.4a, 4A.4b and Figure A-85).

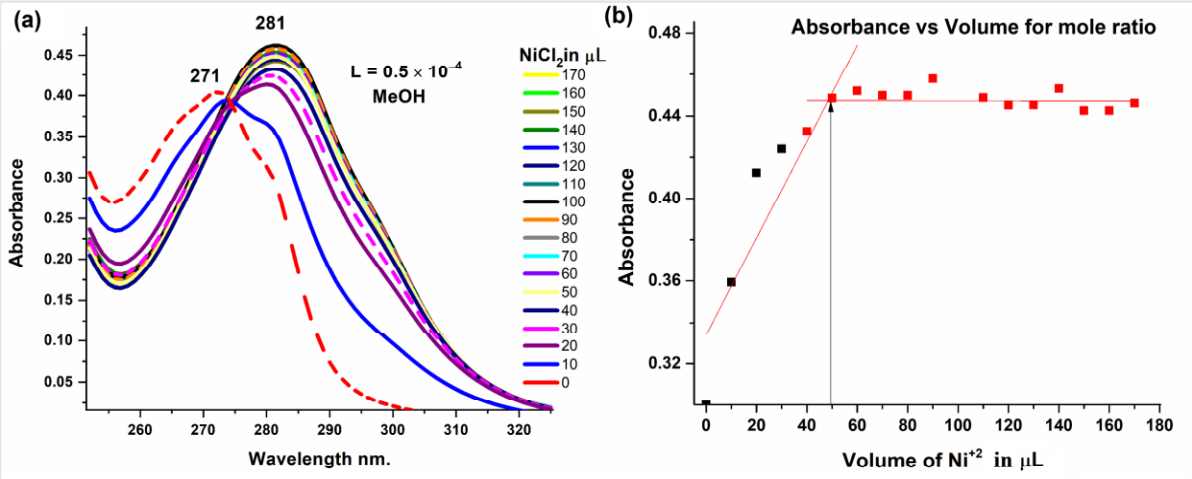

Figure 4A.3: (a) UV-Visible absorption spectra of 1 mL of 0.5×10^{-4} M **L3c** on adding different volume of 10^{-3} M of Ni(II) solution (Total solution volume = 2 mL), (b) Absorbance (of $n \rightarrow \pi^*$ peak) vs. Volume of Ni(II) solution in overall volume of 2 mL solution

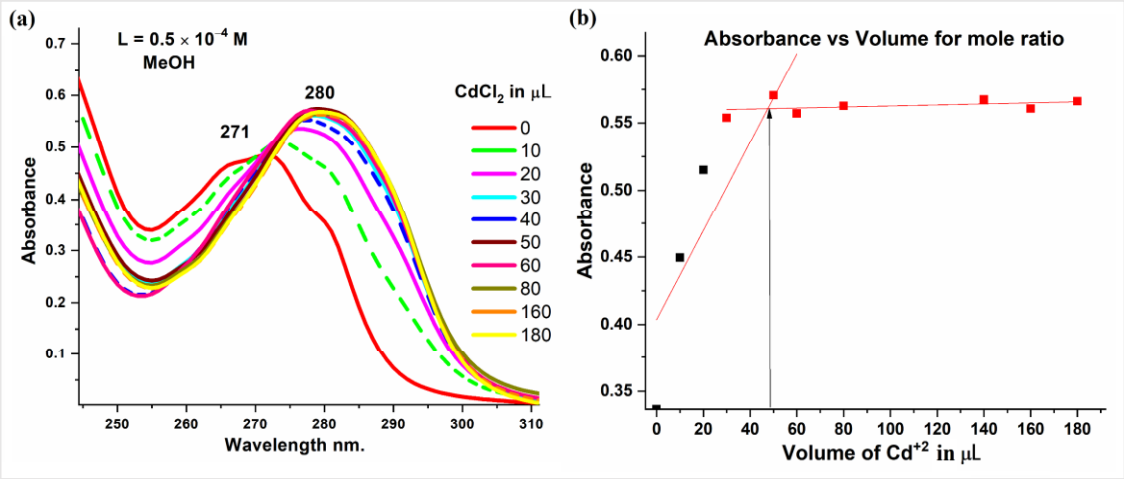

Figure 4A.4: (a) UV-Visible absorption spectra of 1 mL of 0.5 × 10^{-4} M **L3c** on adding different volume of 10^{-3} M of Cd(II) solution (Total solution volume = 2 mL), (b) Absorbance (of n → π* peak) vs. Volume of Cd(II) solution in overall volume of 2 mL solution

4A.3.4 Yoe Jones method for calculating binding constant of Cd(II) and Ni(II) with L3c

The binding constant of Ni(II) and Cd(II) with **L3c** was calculated using Yoe Jones Method from a non-linear least squares fit analysis method at 281 nm (Figure 4A.5). The reaction of formation of the complex can be written as $M_mL_n \leftrightarrow mM + nL$, where M = metal ion, L = ligand and m, n = corresponding stoichiometric coefficient. The equation of dissociation of the complex and stability can be expressed as;

$$M_mL_n \quad \leftrightarrow \quad mM + nL$$

C	0	0	Initial concentration
$(1-\alpha)C$	$m\alpha C$	$n\alpha C$	Equilibrium concentration

$$K = \frac{(1-\alpha)C}{m(\alpha C)^m(n\alpha C)^n} \qquad \rightarrow(1)$$

According to Beer-Lambert's law

$$A_\alpha = \epsilon . b(\alpha C) \qquad \rightarrow(2)$$

$$\alpha = \frac{A_\alpha}{\epsilon b C} \qquad \rightarrow(3)$$

$$A_\alpha = A_0 - A_{max} \qquad \rightarrow(4)$$

where α is the degree of dissociation, C = concentration, b is the path length.

The binding constant K is found to be 26.88 × 10^6 L/mol for Ni^{+2} (Figure 4A.6) and 4.29 × 10^6 L/mol for Cd^{+2} respectively (Figure A-86 to A-87, which includes the calculation part).

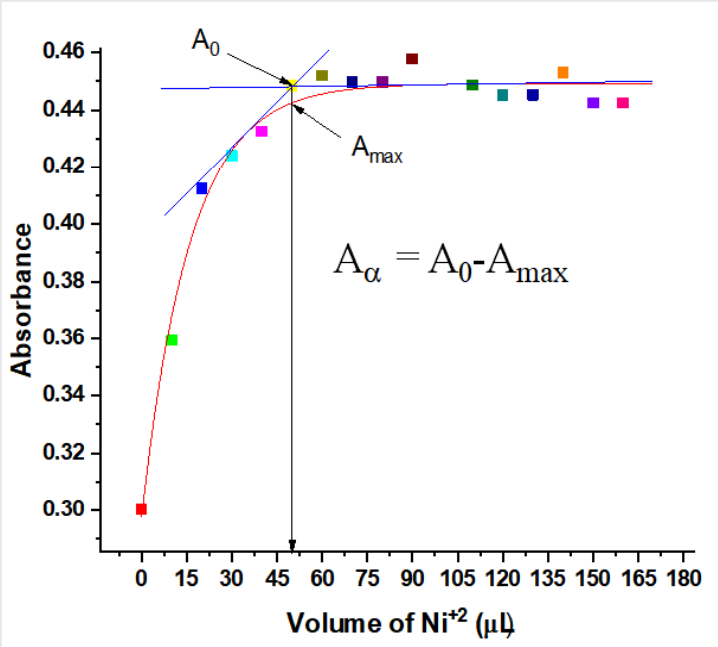

Figure 4A.5: (a) Determination of binding constant of Ni^{+2} with **L3c** from Yoe Jones Method using non-linear least square fit analysis method at 281 nm

For Ni^{+2}

$$A_\alpha = A_0 - A_{max} \quad (4)$$

$$A_\alpha = 0.4482 - 0.4419$$

$$A_\alpha = 0.0063$$

$$A_\alpha = \epsilon . b(\alpha C) \quad (2)$$

$$\alpha = \frac{A_\alpha}{\epsilon b C} \quad (3)$$

$$\alpha = \frac{0.0063}{0.3304 \times 10^4 \times 1cm \times 10^{-4}}$$

$$\alpha = 0.0191$$

$$K = \frac{(1 - 0.0191) \times 10^{-4}}{(0.0191 \times 10^{-4})(0.0191 \times 10^{-4})}$$

$$K = 26.88 \times 10^6\ M^{-1}$$

Figure 4A.6: Binding constant calculation of **Ni(II)-**L3c complex

4A.3.5 Metal ion sensitivity and selectivity

The detection limit (DL) of **L3c** towards sensing Ni(II) and Cd(II) metal ions is determined by measuring the absorbance of different concentrations of Ni(II) in 1×10^{-5} M of **L3c**. From the plot of absorbance (at 281nm) vs. concentration of Ni(II), the detection limit was calculated to 3.08 μM for Ni(II) using the following equation, DL = (K × Sb1)/S, where K = 3, Sb1 is the

standard deviation of blank that is 0.001224 and S = slope = 0.0012 × 10^6 which is calculated from the graph (absorbance vs concentration) (Figure 4A.7, Figure A-88). A similar procedure was adopted for Cd(II) and it was calculated to be 1.47 μM (Figure A-89 and A-90). The selectivity of **L3c** towards sensing Ni(II) and Cd(II) was determined by measuring the UV-visible absorption spectra of 1:1 ratio of **L3c** and Cd(II) or Ni(II) in presence of four equivalents of other interfering metal ions (Figure A-91). A profile of absorbance at 281 nm for **L3c** and Cd(II) or Ni(II) in presence of different interfering metal ions showed that there is a negligible effect (except iron) in the absorbance of **L3c** and Cd(II) or Ni(II) due to the presence of other interfering metal ions (Figure 4A.8a and 4A.8b).

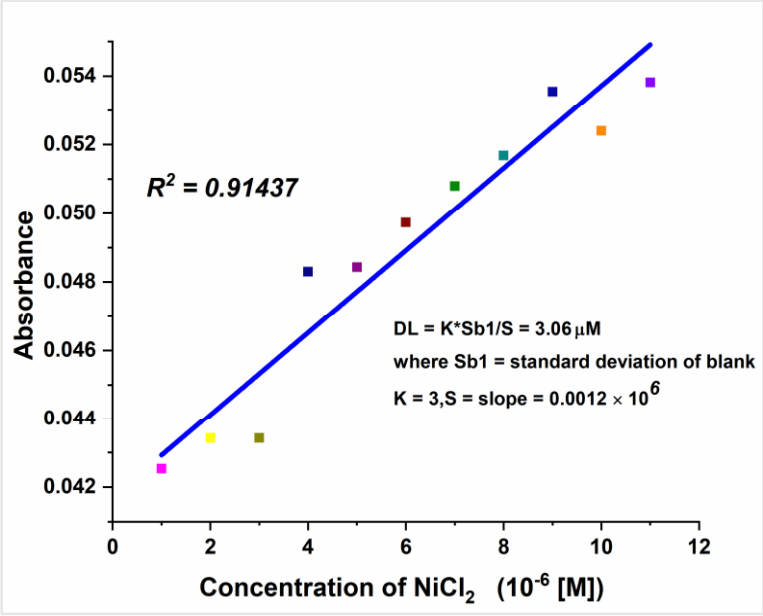

Figure 4A.7: Linear fit of Absorbance (~281nm) vs. Concentration of Ni(II) in 1 × 10^{-5} M of **L3c**

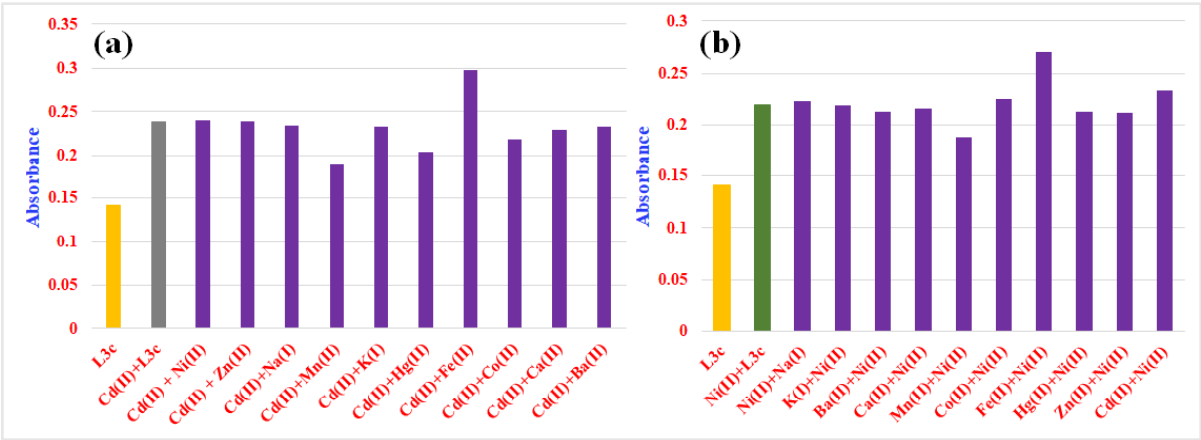

Figure 4A.8: Selectivity of **L3c** towards Ni(II) and Cd(II): (a) Absorbance (281 nm) profile of **L3c** and Ni(II) in presence of four equivalents of interfering M^{+2}; (b) Absorbance (280 nm) profile of **L3c** and Cd(II) in presence of four equivalents of interfering M^{+2}

4A.3.6 To study the size and cavity factor effect on the selection of best sensor among various di-imines

The sensing ability of a compound is dependent on various factors and the geometry that it will attain as a result of complex formation is one of the important attributes. In order to understand the effect of geometry of the complex on the selectivity and sensing ability, the UV-visible absorption of **L2′c**, **L4c,** and **L13c** with various metal ions using methanolic solution were recorded. The UV-visible absorption of **L2′c** was carried out in 1:1 ratio [ligand: metal (v/v), pH ~ 6.94 - 7.68], where 50 μL of **L2′c** and 50 μL of metal ion solution were taken from 10^{-3} M of stock solution of **L2′c** and metal ion solution respectively in a quartz cuvette and made up the final volume 2 mL (Figure 4A.9). Similarly, UV-visible absorption of **L4c** and **L13c** was carried out in 1:2 ratio [ligand: metal (v/v), pH ~ 6.94 - 7.68], where 25 μL of **L4c** or **L13c** and 50 μL of metal ion solution were taken from 10^{-3} M of stock solution of **L4c** or **L13c** and metal ion solution respectively. Figure 4A.9 shows that the compound **L2′c**, **L4c** and **L13c** (Figure A-92) have no selectivity, almost all transition and heavy metals have responded to these spacers.

The possible structure that may result when 1:1 complex formation **L2′c** with metal ions consists of two five membered and one six membered chelate ring which are thermodynamically stable and can accommodate a range of transition and heavy metals (Figure 4A.10 and Figure A-93). In case of **L3c**, the 1:1 complex resulted in the formation of two five membered and one seven membered chelate ring. The seven membered ring may be more selective towards nickel and cadmium over other metal ions. In case of **L4c**, the mole ratio method shows a 1:2 (**L4c**: metal ion) stoichiometry of the complex (Figure A-94). The inability both the imine groups of the sensor molecule to simultaneously chelate the metal ion due to the spacer length (hexyl) is the reason of not forming 1:1 complex, while the 1:2 complex doesn't result in selectivity. The 1:2 complex results in the formation of two five membered rings, which can result from a wide range of transition metal centres irrespective of the size. The 1:1 (**L4c**:metal ion) stoichiometric complex may be thermodynamically unfavourable due to the large spacer length of **L4c,** which may result in a nine membered chelate ring.

In case of **L13c**, the UV-visible absorption spectra indicated the formation of 1:2 complex of **L13c** and metal (**Figure A-92**). The presence of rigid aromatic spacer has eliminated the possibility of chelation and hence the selectivity attained by **L3c** due to chelate was not observed in **L13c**.

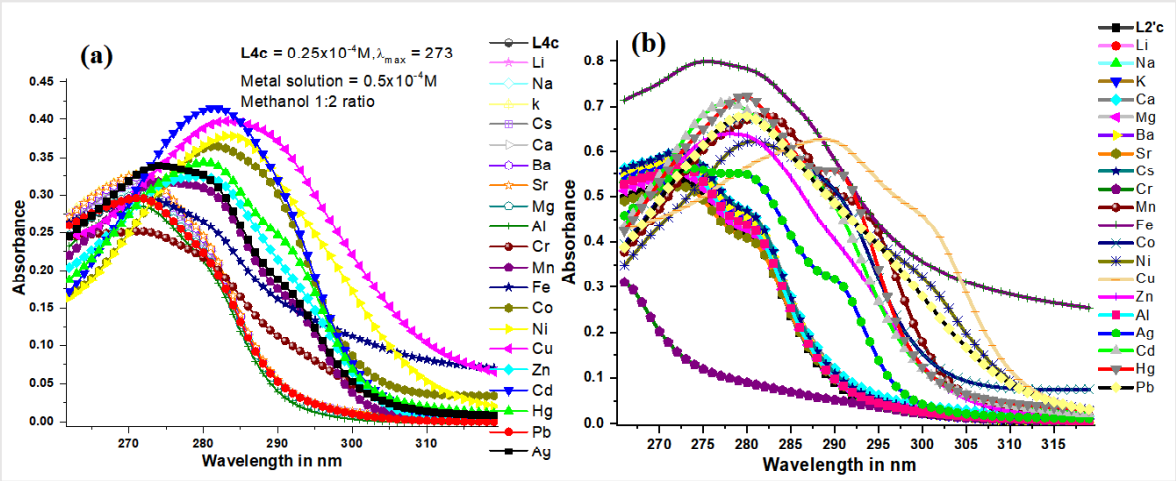

Figure 4A.9: UV-Visible absorption spectra of **L2′c** and **L4c** with different metal ions

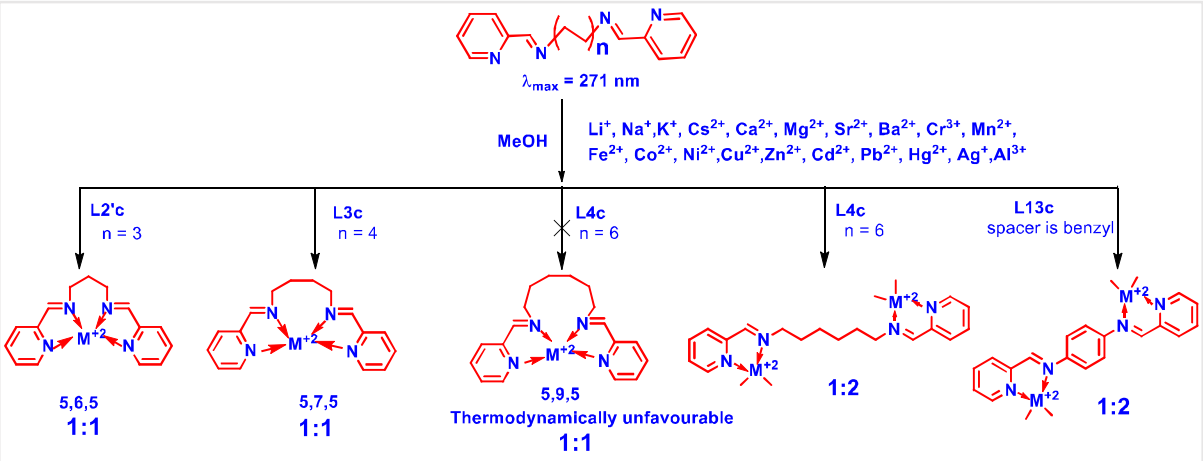

Figure 4A.10: Schematically diagram of possible structure of different di-imines

4A.3.7 Stability of the Ni(II)-L3c complex in presence of various anions

The UV-visible absorption of the **Ni(II)-L3c** complex with various anions was recorded in order to check its stability. The source of anion taken during the experiments were sodium salts, which included NaN_3, $NaBH_4$, NaCl, $NaClO_4$, NaOH, NaS_2O_3, $NaSO_4$, $NaBF_4$, $NaCO_3$, and potassium salts KSCN, KF. Figure 4A.11b shows that absorbance of the complex is almost constant in methanol and water respectively and the stability of the complex is unchanged in presence of various anions.

4A.3.8 pH study

The pH sustainability of **L3c** sensor was analysed using buffer solution (CH_3COOH and CH_3COONa) in the range of 3.72-5.57 (Figure A-95). A 1:1 10^{-3} M **Ni(II)-L3c** solution was prepared for the pH study, after that, 50 μL of 10^{-3} M solution of **Ni(II)-L3c** was added to 1.95 mL of buffer solution then final concentration of the solution became 0.25×10^{-4} M and the

absorbance was recorded. The λ_{max} corresponding to the absorption spectra of **Ni(II)-L3c** increases linearly with increase in pH from 3.72 to 5.57 (Figure 4A.11a).

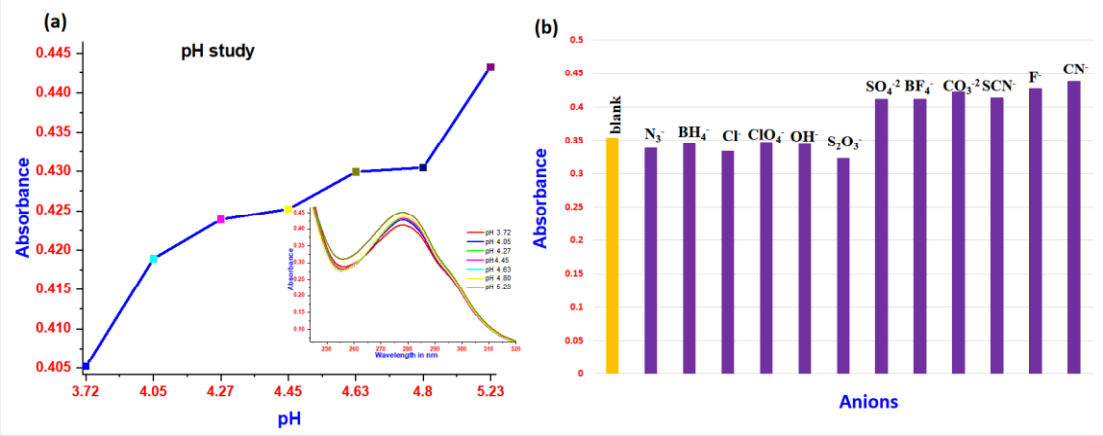

Figure 4A.11: (a) The pH study of **Ni(II)-L3c** complex at 281 nm and inside image represents their corresponding spectra (b) Stability of **Ni(II)-L3c** complex with various anions at 281 nm and their absorbance profile

4A.3.9 Complexation study by several techniques

Due to lack of crystal structure of **Cd(II)- L3c**, NMR, PXRD, FESEM and EDS analysis have been performed to prove the complexations.

4A.3.9.1 Binding mode of L3c with Ni(II) from PXRD

In order to understand the binding mode of Ni(II) with **L3c**, the 1:1 complex of **L3c** with $NiCl_2$ was synthesized. Mendoza et al., have reported the crystal structure of the complex of **L3c** and $NiCl_2$.[41]

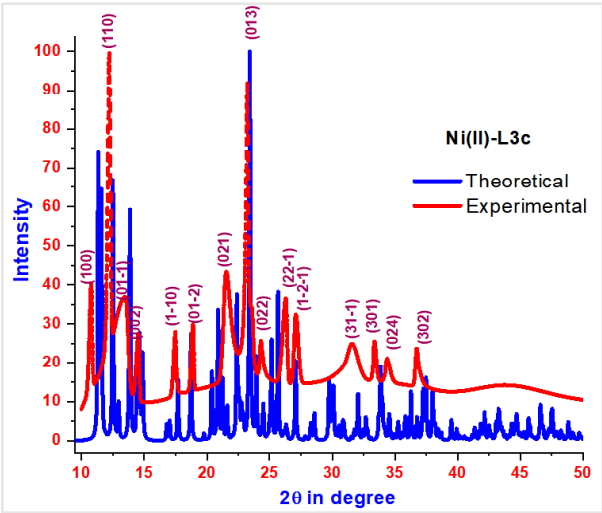

Figure 4A.12: PXRD of **Ni(II)-L3c** complex; Simulated PXRD generated from crystal data CCDC no. 1043600 (blue line); Experimental PXRD of synthesized **L3c**-Ni(II) complex (red line)

The powder XRD of the synthesized complex was compared with the simulated powder XRD with the report-structure (Figure 4A.12). From the powder XRD of the complex of **Ni(II)-L3c,** *h*, *k*, *l* values are determined from each of the peaks (2θ). The reflection planes of **Ni(II)-L3c** complex are 100, 110, 01–1, 002, 0–10, 01–2, 021, 013, 022, 22–1, 1–2–1, 31–1, 301, 024, 302, which refer to the angle of 10.77, 12.20, 13.4, 14.44, 17.47, 18.91, 21.63, 23.13, 24.42, 26.33, 27.29, 31.68, 33.36, 34.48, 36.71, respectively.

The previous reports of single crystal XRD of **L3c** and its Ni(II) complex was also analysed to get an insight of the structural features of the compounds leading to an understanding of the reason behind the good binding constant of Ni(II) with **L3c**.

4A.3.9.2 NMR studies to elucidate binding of L3c to Cd (II)

The NMR spectra of **L3c** were recorded in DMSO-d_6. In order to assign each aromatic proton peaks, COSY (Figure A-96) and Selective NOE (Figure A-97) were performed. The ^{1}H-NMR of 1:1 solution of **L3c** and $CdCl_3$ showed deshielding of protons *ortho* and *para* to pyridyl nitrogen (proton p and r in Figure 4A.13). The deshilding of the imine hydrogen was also observed (Proton t in Figure 4A.13). This indicated the complex formation of **L3c** with Cd^{+2}. As the molar ratio of **L3c** and Cd^{+2} was changed from 1:1 to 1:2, the protons p, r and t became more deshielded. However, on recording the spectra of 1:2 molar ratio of **L3c** and Cd^{+2} after 24 h, it was observed that the peak positions shifted and matched the peak position of 1:1 complex (Figure 4A.13). This infers that the 1:2 complex may not be thermodynamically stable and changed to stable 1:1 complex on standing for long time.The similar study has been done in the presence of Ca^{+2} ion, but no change in the NMR of **L3c** was observed (Figure A-98).

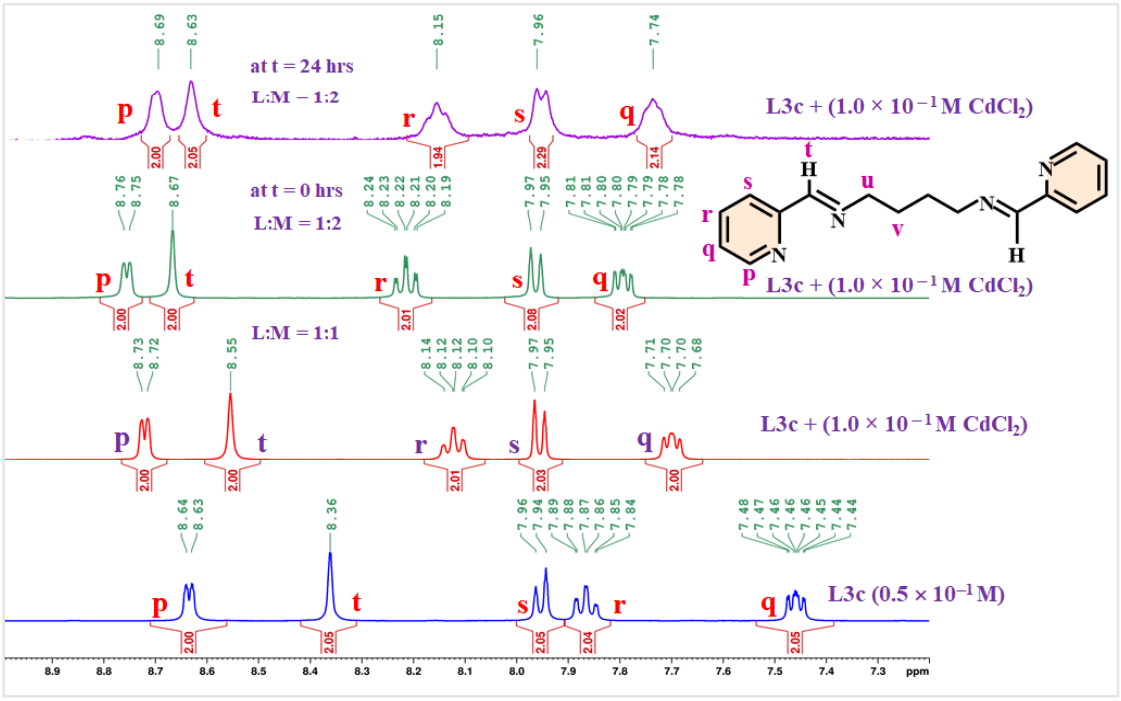

Figure 4A.13: ^{1}H-NMR spectra (a) **L3c**, (b) 1:1 (**L3c**:Cd(II)), (c) at t = 0 h, 1:2 (**L3c**: Cd(II)) and (d) at t = 24 h, (**L3c**:Cd)

4A.3.9.3 Structural description of the complex of L3c with $NiCl_2$

The crystal structure of **L3c** was reported previously by our group. It is crystallized in monoclinic $P2_1/c$ space group and the asymmetric unit contains half of the molecule. The

overall "S" shaped geometry of the molecule is mainly due to the butyl chain *gauche-anti-gauche* conformation (Figure 4A.14a). It is important to note here that the imine hydrogen is involved in C–H···N hydrogen bond interaction with pyridyl-N. The compound **L3c** was shown to have enhanced emission in the solid state, which was attributed to the formation of a "non-covalently bonded chromophore" unit (Figure 4A.14a).

The crystal structure analysis of the complex of **L3c** with $NiCl_2$ was done by Pioquinto-Mendoza and coworkers. The complex is crystallized in triclinic $P\bar{1}$. Ni(II) has a distorted octahedral geometry with two pyridyl N, two imine N, one Cl^- and one H_2O satisfying the coordination environment, while one more Cl^- remained uncoordinated to the Ni(II) centre (Figure 4A.14b (p)). The geometry of the ligand, **L3c**, in the complex is twisted and bent where the butyl chain adopted *gauche-gauche-gauche* conformation. It should also be noted that a strong O–H···Cl^- hydrogen bond interaction (2.37(3) Å, 3.1394(19) Å, 163(3)°; 2.32(3) Å, 3.0947(17) Å, 176(3)°) is present between the water molecules and the uncoordinated Cl^- anions, which are connecting the two adjacent **L3c** -Ni(II) complex molecules. The coordinated Cl^- is also involved in hydrogen bond interaction with imine H (N=C–H···Cl^-: 2.61 Å, 3.405(2) Å, 144°; 2.73 Å, 3.481(3) Å, 138°; 2.68 Å, 3.594(3) Å, 166°) (Figure 4A.14b (q)). The 3D arrangement of the complex molecules shows the arrangement of pyridyl rings in parallel slipped manner (centroid-to-centroid distance of 3.936 Å) and parallel offset manner (centroid-to-centroid distance of 4.903 Å) (Figure 4A.14b (r)). The complex has a 1:1 ratio of Ni(II) and **L3c**. The formation of a chelate type complex with Ni(II) is responsible for a good binding constant that is observed for **L3c** in sensing Ni(II).

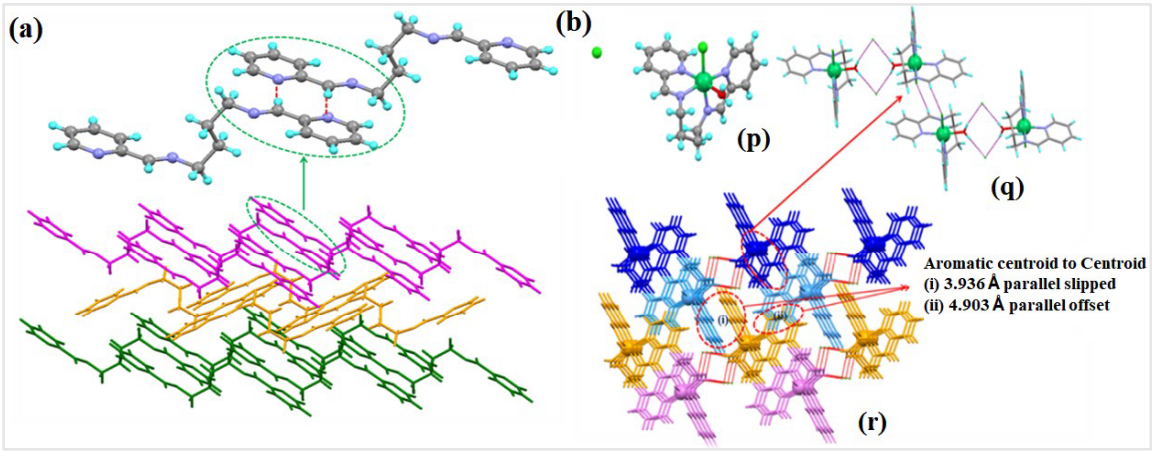

Figure 4A.14: (a) Illustration of crystal structure of **L3c**; Notice the gauche-anti-gauche conformation of butyl chain and C–H●●●N interactions to form non-covalent chromophore moiety; Figures were generated from the data obtained from CCDC no. 930055 **(b):** Illustration of crystal structure of **L3c**-Ni(II): (p) Asymmetric unit; (q) O-H●●●Cl- and N=C-H●●●Cl- hydrogen bond interactions between the **L3c**-Ni(II) molecules; (r) 3D packing of the molecules; Notice the arrangement of the aromatic rings; Figures were generated from CCDC no. 1043600

4A.3.9.4 FE-SEM and EDS analysis of Cd(II)-L3c and Ni(II)-L3c

FE-SEM analysis of **Cd(II)-L3c**, **Ni(II)-L3c,** and **L3c** have been done for checking morphology difference between 1:1 **Cd(II)-L3c**, 1:1 **Ni(II)-L3c** and **L3c**. The morphology of **L3c** showed quenched stone like structure is transformed into fairly sprinkled elliptical shape like structure after addition of cadmium ion. But the nickel(II) addition gave scattered broken sheet like structure. Electron Disperse Spectroscopy of **Cd(II)-L3c**, clearly showed the peak of carbon(C), nitrogen(N), oxygen(O), chlorine(Cl), and cadmium(Cd), elements (Figure 4A.15).

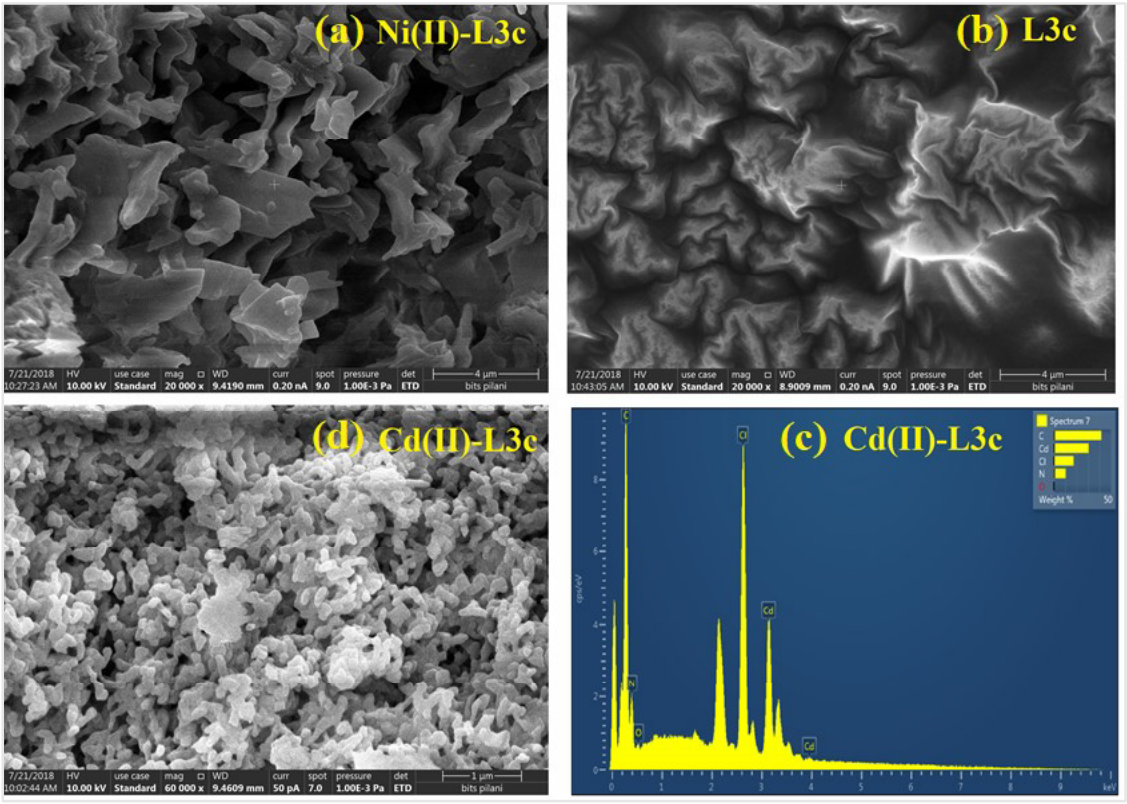

Figure 4A.15: SEM analysis of (a) **Ni(II)-L3c**, (b) **L3c** and (d) **Cd(II)-L3c** and (c) EDS analysis of **Cd(II)-L3c**

4A.3.10 Real time experiment

The presence of nickel ions in environmental samples was determined to examine the real time application of the **L3c** sensor. The water sample from river water (collected from Ganga river at Kolkata Aahirotola) was analyzed by atomic absorption spectroscopy (AAS) and 1.2414 ppm of Ni^{+2} ion was detected directly in river water (Table 4A.1). For verifying the effectiveness of **L3c** in detecting Ni(II) from the river water sample, 100–500 μM concentration of nickel ion was spiked into river water and **L3c** was added to this solution. **L3c** detects nickel ion at micro molar level and due to this reason, nickel ions were spiked in the river water sample. Table 4A.1 showed the amount of Ni(II) detected by using **L3c**. Figure A-

80 and Figure A-81 shows standard calibration graph for nickel ions and river water sample (spiked river water sample) respectively (the detailed procedure is included in the experimental section). The AAS of spiked river water sample showed the presence of 1.3529 ppm of Ni^{+2} (Table 4A.1).

Table 4A.1: Determination of Ni^{+2} ion

Determination of Ni^{+2} ion in river water using AAS analysis				Determination of Ni^{+2} ion in river water sample using **L3c** receptor				
Sample	True value	Conc. (ppm)	Absorbance	Metal ions (μM)	Added	Found	Recovery, %	RSD, %
STD 1	1 ppm	0.9688	0.0290	Ni^{+2} in Ganga Jal	100	164	164	0.063
STD 2	2 ppm	1.9370	0.0837	Ni^{+2} in Ganga Jal	200	269	134.5	0.017
STD 3	3 ppm	3.1104	0.1500	Ni^{+2} in Ganga Jal	300	361	120.33	0.146
STD 4	4 ppm	4.0927	0.2055	Ni^{+2} in Ganga Jal	400	442	110.5	0.054
STD 5	5 ppm	4.8910	0.2506	Ni^{+2} in Ganga Jal	500	503	100.6	0.128
River water	unknown	1.2414	0.0444					
River+Std	unknown	1.3529	0.0474					

4A.3.11 Comparison of L3c with other representative sensors

The comparison of **L3c** with different well reported nickel sensor is shown in Figure 4A.16 and Table A-6. Prabhu et al.,[23] have established a chalcone based fluorescent chemosensor for nickel which has a detection limit up to micro molar level (5.14 μM) and binding constant is 1.91 × 10^5 M^{-1} (Figure 4A.16a). Domínguez et al.,[39] have reported colorimetric nickel sensor based on novel Schiff base derivative from cinnamaldehyde, detection limit 0.1 μM and binding constant is 1.29 × 10^5 M^{-1} (Figure 4A.16b). Amini et al., Have reported[40] optical nickel sensor from azo compound using Nafion membrane (Figure 4A.16c). Goswami et al., have derived nickel sensors from quinoxaline derivative[11a, 41] and determined the binding constant 1.26 × 10^5 M^{-1} (Figure 4A.16d) and 2.5 × 10^5 M^{-1} (Figure 4A.16f). Jiang et al., have reported coumarin based colorimetric nickel sensor[29] with a low binding constant 2.343 × 10^4 M^{-1}

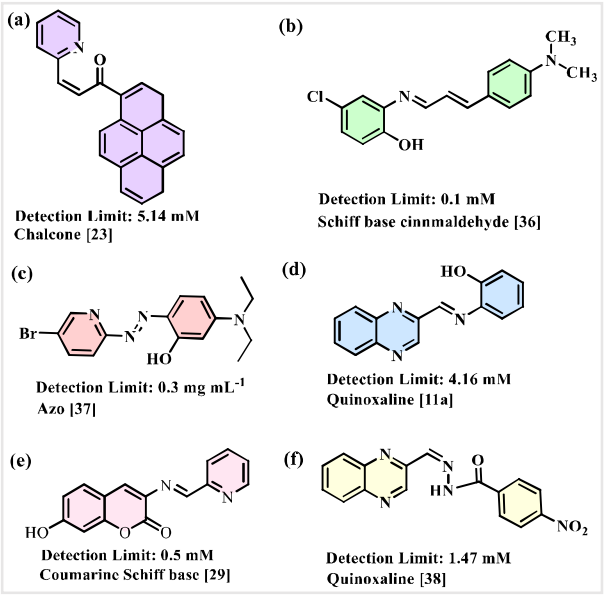

Figure 4A.16: Some other Imine and Azo based Ni^{2+} sensor with their detection limit reported in literature[11a, 23, 29, 36-38]

(Figure 4A.16e). In the present work, the detection limit of nickel (10^{-6} [M]) is lower than the maximum contaminant level goal (MCLG = 1.7×10^{7} M), which is provided by American Environmental Protection Agency (AEPA) for Ni^{+2} in drinking water. The comparison table for cadmium is shown in appendix (Table A-7).

4A.4 Conclusions

A di-Schiff base ligand, **L3c**, was observed to function as a ratiometric chemosensor for Ni^{+2} and Cd^{+2} ions. The sensitivity of **L3c** in detecting Ni^{+2} and Cd^{+2} was at micro molar level. **L3c** was also selective in detecting the two ions because of its high tolerance level in presence of other interfering metal ions. The 1:1 binding mode of Ni^{+2} and Cd^{+2} with **L3c** was calculated using the mole ratio method, which was verified by the reported nickel complex crystal structure, ^{1}H-NMR analysis of cadmium complex and FE-SEM analysis. **L3c** was also used in determining the Ni^{+2} from a river water sample.

4A.5 References

[1] (a) Tchounwou P. B., Yedjou C. G., Patlolla A. K., Sutton D. J., *Molecular, Clinical and Environmental Toxicology: Volume 3: Environmental Toxicology*. Springer Basel; **2012**:133-164; (b) Nordberg G. F., Fowler B. A., Nordberg M., *Handbook on the Toxicology of Metals (Fourth Edition)*. Academic Press; **2015**:1-12.

[2] Flowers G. E., Kelly Jr E. L., Grossklaus Jr W. D., Barber J. D., Grubbs G. W., Williams L. Elevated-temperature, plasma-transferred arc welding of nickel-base superalloy articles. 2000: Google Patents; **2000**.

[3] Krämer U., Clemens S., *Molecular Biology of Metal Homeostasis and Detoxification: From Microbes to Man*. Springer Berlin Heidelberg; **2006**:215-271.

[4] Wang L., Ye D., Cao D., *Spectrochim. Acta, Part A,* **2012**, 90, 40-44.

[5] Wang Z., Palacios M. A., Anzenbacher Jr P., *Anal. Chem.,* **2008**, 80(19), 7451-7459.

[6] Spichiger-Keller U. E. *Chemical Sensors and Biosensors for Medical and Biological Applications*. Weinheim: Wiley-VCH; 2008.

[7] Haase O., Klare M., Broekaert J. A., Krengel-Rothensee K., *Analyst,* **1998**, 123(6), 1219-1222.

[8] Zendelovska D., Pavlovska G., Cundeva K., Stafilov T., *Talanta,* **2001**, 54(1), 139-146.

[9] de Torres A. G., Pavón J. M. C., Castellon E. R., *J. Anal. At. Spectrom.,* **1998**, 13(4), 243-248.

[10] (a) Zhao Q., Li R.-F., Xing S.-K., Liu X.-M., Hu T.-L., Bu X.-H., *Inorg. Chem.,* **2011**, 50(20), 10041-10046; (b) Goswami S., Manna A., Aich K., Paul S., *Chem. Lett.,* **2012**, 41(12), 1600-1602; (c) Goswami S., Aich K., Das S., Das Mukhopadhyay C., Sarkar D., Mondal T. K., *Dalton Trans.,* **2015**, 44(12), 5763-5770.

[11] (a) Goswami S., Chakraborty S., Das A. K., Manna A., Bhattacharyya A., Quah C. K., Fun H.-K., *RSC Adv.,* **2014**, 4(40), 20922-20926; (b) Goswami S., Paul S., Manna A., *RSC Adv.,* **2013**, 3(47), 25079-25085.

[12] (a) Goswami S., Das A. K., Aich K., Manna A., Maity S., Khanra K., Bhattacharyya N., *Analyst,* **2013**, 138(16), 4593-4598; (b) Goswami S., Maity S., Maity A. C., kumar Das A., Pakhira B., Khanra K., Bhattacharyya N., Sarkar S., *RSC Adv.,* **2015**, 5(8), 5735-5740; (c) Goswami S., Sen D., Das A. K., Das N. K., Aich K., Fun H.-K., Quah C. K., Maity A. K., Saha P., *Sens. Actuators, B,* **2013**, 183, 518-525.

[13] (a) Wang W., Zhang Y.-m., Li Y.-x., Zhao Q., *Chem. Res. Chin. Univ.,* **2013**, 29(4), 632-637; (b) Aich K., Goswami S., Das S., Mukhopadhyay C. D., Quah C. K., Fun H.-K., *Inorg. Chem.,* **2015**, 54(15), 7309-7315; (c) Goswami S., Aich K., Das S., Das A. K., Manna A., Halder S., *Analyst,* **2013**, 138(6), 1903-1907.

[14] (a) Gupta V. K., Kumar P., *Anal. Chim. Acta,* **1999**, 389(1), 205-212; (b) Gupta V. K., Prasad R., Kumar P., Mangla R., *Anal. Chim. Acta,* **2000**, 420(1), 19-27.

[15] Gupta V., Singh A., Gupta B., *Anal. Chim. Acta,* **2007**, 583(2), 340-348.

[16] Gupta V. K., Prasad R., Kumar A., *Sensors,* **2002**, 2(10), 384-396.

[17] Gupta V. K., Singh A. K., Pal M. K., *Anal. Chim. Acta,* **2008**, 624(2), 223-231.

[18] Gupta V. K., Goyal R. N., Agarwal S., Kumar P., Bachheti N., *Talanta,* **2007**, 71(2), 795-800.

[19] Cao Y. W., Li X. L., He Y. W., *Eur. J. Chem.,* **2017**, 8(3), 314-316.

[20] Aksuner N., Henden E., Yilmaz I., Cukurovali A., *Sens. Actuators, B,* **2012**, 166, 269-274.

[21] Gupta V. K., *Int. J. Electrochem. Sci,* **2015**, 10, 7854-7865.

[22] Dodani S. C., He Q., Chang C. J., *J. Am. Chem. Soc.,* **2009**, 131(50), 18020-18021.

[23] Prabhu J., Velmurugan K., Raman A., Duraipandy N., Kiran M. S., Easwaramoorthi S., Nandhakumar R., *Sens. Actuators, B,* **2017**, 238, 306-317.

[24] Goswami S., Chakraborty S., Adak M. K., Halder S., Quah C. K., Fun H.-K., Pakhira B., Sarkar S., *New J. Chem.,* **2014**, 38(12), 6230-6235.

[25] Wang J., Jiang C., Wang X., Wang L., Chen A., Hu J., Luo Z., *Analyst,* **2016**, 141(20), 5886-5892.

[26] Bao Y., Liu B., Wang H., Du F., Bai R., *Anal. Methods,* **2011**, 3(6), 1274-1276.

[27] Li L., Dang Y.-Q., Li H.-W., Wang B., Wu Y., *Tetrahedron Lett.,* **2010**, 51(4), 618-621.

[28] Li G.-B., Fang H.-C., Cai Y.-P., Zhou Z.-Y., Thallapally P. K., Tian J., *Inorg. Chem.,* **2010**, 49(16), 7241-7243.

[29] Jiang J., Gou C., Luo J., Yi C., Liu X., *Inorg. Chem. Commun.,* **2012**, 15, 12-15.

[30] Baig F., Kant R., Gupta V. K., Sarkar M., *RSC Adv.,* **2015**, 5(63), 51220-51232.

[31] Pioquinto-Mendoza J. R., Rosas-Ortiz J. A., Reyes-Martínez R., Conelly-Espinosa P., Toscano R. A., Germán-Acacio J. M., Avila-Sorrosa A., Baldovino-Pantaleón O., Morales-Morales D., *Inorg. Chim. Acta,* **2015**, 438, 146-152.

[32] Keypour H., Zebarjadian M. H., Rezaeivala M., Shamsipur M., Sabounchei S. J., *J. Iran. Chem. Soc.,* **2013**, 10(6), 1137-1143.

[33] Cheng J., Wei K., Ma X., Zhou X., Xiang H., *J. Phys. Chem. C,* **2013**, 117(32), 16552-16563.

[34] Yoe J. H., Jones A. L., *Ind. Eng. Chem., Anal. Ed.,* **1944**, 16(2), 111-115.

[35] Campbell T. G., Urbach F. L., *Inorg. Chem.,* **1973**, 12(8), 1836-1840.

[36] Sadajiro Y., Hiroshi I., **1954**, *JP 29003480 B*.

[37] Wu H.-C., Thanasekaran P., Tsai C.-H., Wu J.-Y., Huang S.-M., Wen Y.-S., Lu K.-L., *Inorg. Chem.,* **2006**, 45(1), 295-303.

[38] Zolezzi S., Decinti A., Spodine E., *Polyhedron,* **1999**, 18(6), 897-904.

[39] Peralta-Domínguez D., Rodríguez M., Ramos-Ortíz G., Maldonado J. L., Meneses-Nava M. A., Barbosa-García O., Santillan R., Farfán N., *Sens. Actuators, B,* **2015**, 207, 511-517.

[40] Amini M. K., Momeni-Isfahani T., Khorasani J. H., Pourhossein M., *Talanta,* **2004**, 63(3), 713-720.

[41] Goswami S., Chakraborty S., Paul S., Halder S., Maity A. C., *Tetrahedron Lett.,* **2013**, 54(37), 5075-5077.